Available online at www.sciencedirect.com
SCIENCE DIRECT®
Journal of the European Ceramic Society 25 (2005) 1863–1876
www.elsevier.com/locate/jeurceramsoc

Crystal structures of CeO_2–ZrO_2–Ta_2O_5 ternary system studied by Rietveld method

Dore Augusto Clemente, Elio Lucchini*, Sergio Meriani, Noella Furlan

Department of Materials Engineering and Applied Chemistry, University of Trieste, Via Valerio 2, 34127 Trieste, Italy

Received 23 April 2004; received in revised form 7 June 2004; accepted 20 June 2004
Available online 28 August 2004

Abstract

Solid solutions of the pseudo-ternary system $Ce_{0.6/(1+x)}Zr(Hf)_{(0.4-x)/(1+x)}Ta_{2x/(1+x)}$ ($0.00 \leq x \leq 0.06$), i.e. having molecular composition 1, 2, 3, 4, 5 and 6% in Ta_2O_5, have been prepared by traditional ceramic methods (1500 °C for 3 h). SEM observations and analysis of the X-ray diffraction powders allowed to establish that the solubility of Ta_2O_5 in the above mentioned system is 4 %mol. The Rietveld analysis of the powder X-ray diffraction data has shown that all the samples of the solid solution crystallize in tetragonal space group $P4_2/nmc$ (No. 137) but are nearly cubic, space group $Fm\bar{3}m$ (No. 225). The freshly prepared specimens (from 1 to 4 %mol of Ta_2O_5) show additional peaks due to a tetragonal supercell and also to a modulated structure. However, the modulated peaks disappear after 8 months. Compositions containing 5 and 6% of Ta_2O_5 show also additional peaks due to a small quantity of two crystalline phases having approximate composition: ZrO_2–$2CeO_2$–Ta_2O_5 and $2CeO_2$–Ta_2O_5 (later on identified as $CeTaO_4$).

Keywords: Rietveld analysis; CeO_2; Ta_2O_5; Phase analysis

1. Introduction

ZrO_2–CeO_2 solid solutions and the relative phase diagram were studied through many techniques.[1–21] However, in spite of these efforts, many discrepancies persist in the literature.[18–21] The crystallography of the ZrO_2–CeO_2 system is still a matter of debate.[1–10] A common practice describe the tetragonal structure ($P4_2/nmc$) with a double cell, thus it is transformed into a face-centered tetragonal cell. Such a transformation emphasizes the connection with the fluorite structure, in fact this double cell has $a = a_t\sqrt{2}$, $b = b_t\sqrt{2}$ and $c = c_t$. This practice is unsuitable in X-ray refinement using least-squares method because the use of a supercell leads to high correlations and near-singularities in the refinement procedure,[22] thus it is necessary to use the true space group ($P4_2/nmc$) and to introduce the concept of tetragonality (T) that is defined by Howard and Hunter[23] as $T = c_t/(a_t\sqrt{2})$.

Moreover, according to recent investigations,[20,21] and to our results, there are three different tetragonal forms called t, t' and t'', all having space group $P4_2/nmc$ (No. 137). The t form is the stable form at high temperature, has a low CeO_2 content (20–40 mol%), is transformable into the monoclinic form and has a tetragonality greater than 1.00; t' is a metastable form even at high temperature, has high CeO_2 contents (40–65 mol%) and a tetragonality greater than 1.00; t'' is an intermediate form between t' and the *cubic-phase* and has tetragonality equal to 1.00 but it presents the oxygen atom displaced from 0.5000. Then, it is difficult to distinguish between the t'' and the cubic form because there is no splitting of the peaks, while this is possible with the Rietveld method since we should obtain $a_t\sqrt{2} = c_t$ but a displacement of the oxygen atom from $z = 0.5000$, this is indeed one of the major difficulties encountered in this investigation.

* Corresponding author.
E-mail address: lucchini@univ.trieste.it (E. Lucchini).

0955-2219/$ – see front matter © 2004 Elsevier Ltd. All rights reserved.
doi:10.1016/j.jeurceramsoc.2004.06.002

Moreover Howard and Hunter[23] have proposed a linear relation between δ (the oxygen parameter shift) and the tetragonality T:

$$\delta = 0.24\sqrt{1 - \left(\frac{1}{T}\right)^2} \quad (1)$$

where Tmust be $\geq$1.000. This relation will be used to calculate δ. We must note that if T = 1.00 then δ = 0.00, i.e. no oxygen shift is possible without deformation of the cubic cell, therefore a t'' phase would not be possible.

Introduction of ZrO_2 into a solid solution with CeO_2 favours the NO decomposition in the automotive three-way catalyst converters because ZrO_2 promotes the reduction of CeO_2 to Ce_2O_3. The reduced ceramic support enhances the effectiveness of the Rh catalyst in the NO decomposition and probably participates directly to the NO conversion.[24–28]

The Ce^{3+} ions associated with oxygen vacancies have been suggested as promoting sites for the above mentioned reaction,[24–28] therefore it was decided to incorporate Ta_2O_5 into the ZrO_2–CeO_2 solid solution in order to stabilize a higher quantity of Ce^{3+}. The solid solution containing CeO_2 (60 mol%) and ZrO_2 (40 mol%) was chosen because it appears very effective in the NO conversion and it exhibits, in an appropriate atmosphere and in the presence of supported rhodium, a high reducibility.[24–28]

2. Experimental

2.1. Preparation of the samples

ZrO_2 monoclinic crystalline powder (ZrO_2 97.5% and HfO_2 2.0%, Unitec Ceramics), CeO_2 (99.9%, Fisher) and Ta_2O_5 (99.0%, Aldrich), were used as arrived being in the same form employed in the industrial practice. Appropriate quantities of the starting powders were mixed in an agate planetary mill for 8 h as wet (ethanol) slurries. After drying they were pressed into small cylinders (diameter and height = 1 cm) at 200 MPa and fired, on a platinum strip, for 3 h at 1500 °C in a $MoSi_2$ electric furnace. The heating and cooling rates were of 5 °C/min. The sintering temperature was decided on the basis of preliminary tests, which showed the presence of a liquid phase in the richest Ta_2O_5 composition at temperature above 1630 °C and an incomplete reaction between the oxides at a temperature of 1400 °C. After firing, the sample containing only ceria and zirconia showed a pale yellow colour, whereas all specimens containing also Ta_2O_5 had a dark-green colour that is a clear evidence of the Ce^{3+} presence.

The samples relative density, measured with a helium pychnometer (Carlo Erba DP 110 RC), ranged from 92% (ceria-zirconia composition) to 98% (composition containing Ta_2O_5 3 %mol). The sintered samples were crushed and ground in an agate mortar.

We have decided to study the seven specimens having the following molecular composition (mol%):

Specimen no. 1	CeO_2 (60.00%)–ZrO_2 (39.22%)–HfO_2 (0.78%)
Specimen no. 2	CeO_2 (60.00%)–ZrO_2 (38.24%)–HfO_2 (0.76%)–Ta_2O_5 (1.00%)
Specimen no. 3	CeO_2 (60.00%)–ZrO_2 (37.25%)–HfO_2 (0.75%)–Ta_2O_5 (2.00%)
Specimen no. 4	CeO_2 (60.00%)–ZrO_2 (36.27%)–HfO_2 (0.73%)–Ta_2O_5 (3.00%)
Specimen no. 5	CeO_2 (60.00%)–ZrO_2 (35.29%)–HfO_2 (0.71%)–Ta_2O_5 (4.00%)
Specimen no. 6	CeO_2 (60.00%)–ZrO_2 (34.31%)–HfO_2 (0.69%)–Ta_2O_5 (5.00%)
Specimen no. 7	CeO_2 (60.00%)–ZrO_2 (33.33%)–HfO_2 (0.67%)–Ta_2O_5 (6.00%)

while the nominal compositions of the seven specimens is:

Specimen no. 1	$Ce_{0.60000}Zr_{0.39216}Hf_{0.00784}O_2$
Specimen no. 2	$Ce_{0.59406}Zr_{0.37857}Hf_{0.00757}Ta_{0.01980}O_{2.00990}$
Specimen no. 3	$Ce_{0.58824}Zr_{0.36524}Hf_{0.00730}Ta_{0.03922}O_{2.01961}$
Specimen no. 4	$Ce_{0.58252}Zr_{0.35218}Hf_{0.00704}Ta_{0.05826}O_{2.02913}$
Specimen no. 5	$Ce_{0.57692}Zr_{0.33937}Hf_{0.00679}Ta_{0.07692}O_{2.03846}$
Specimen no. 6	$Ce_{0.57143}Zr_{0.32680}Hf_{0.00654}Ta_{0.09524}O_{2.04762}$
Specimen no. 7	$Ce_{0.56604}Zr_{0.31447}Hf_{0.00629}Ta_{0.11321}O_{2.05660}$

2.2. Thermogravimetric measurements

Thermogravimetric measurements were performed in air up to 600 °C with a Netzsch equipment (STA 409) on portions (1 gr.) of the ground materials (heating and cooling rates 10 °C/min). The samples were kept at the highest temperature for 8 h in order to restore their oxygen content.[15,19] The examination of the TG diagrams (corrected for the buoyancy effect) did not reveal a detectable weight gain therefore, it is possible to infer that, during the cooling state of the sintering process, the Ce_2O_3 present at high temperatures[8,9] was largely reoxidized to CeO_2 (the T.G. equipment sensitivity under our working conditions was estimated at near $\pm$1 mg).

2.3. SEM observations

Fragments of the sintered samples were polished, carbon coated and observed with a Scanning Electrons Microscope (SEM) coupled with a EDS device for the chemical analysis.

2.4. X-ray data collection

Prior to XRD measurements the sintered samples were long pressed in an agar mortar to obtain fine microcrystalline powders. The XRD measurements were made at three different sample ages: (i) freshly prepared specimens (≅10 days); (ii) 8 months after the sintering process; and (iii) 51 months after the sintering process. The XRD patterns were collected at 295 K using two different diffractometers:

(i) a Siemens 386-X-AZ diffractometer with nickel-filtered Cu Kα radiation (30 mA, 40 kV). This device was used only for preliminary investigation and the X-ray data were never used in the Rietveld refinements;
(ii) a D5005 X-ray vertical diffractometer (Bragg–Brentano parafocusing geometry) of the Bruker Analytical X-Ray systems equipped with a diffracted beam graphite monochromator and a scintillation counter. The X-ray beam contained Cu Kα1 and Cu Kα2 wavelengths, respectively with $\lambda_{K\alpha1}$ = 1.5406 Å and $\lambda_{K\alpha2}$ = 1.5444 Å and intensity ratio Cu Kα2/Cu Kα1 of 0.5. A divergence slit of 0.6° and a receiving slit of 0.1 mm were used.

The XRD spectra of the 8 months aged compounds, with composition 0, 1 and 2% in Ta_2O_5, were collected with a step-size of 0.02° and a step counting of 5 s and a scan range of 5–140° in 2θ. This combination provides a total of 6501 data points. All the other XRD spectra, except the specimen no. 3, were collected with a scan range of 10–150° in 2θ, a step-size of 0.02° and a step counting of 16 s, this combination provides a total of 7001 data points. For the specimen no. 3: $Ce_{0.58824}Zr_{0.36524}Hf_{0.00730}Ta_{0.03922}O_{2.01961}$ more sophisticated conditions (scan range 10–150° in 2θ, step-size 0.015° and step counting 15 s) were used. This combination provides a total of 9345 data points.

3. Determination of the extent of the solid solution zone

3.1. SEM observations

The analysis of the back-scattered images revealed that the solid solution extends up to composition 5 ($0.00 \leq x \leq 0.04$), whereas for x values above 0.04 (compositions 6 and 7) the presence of a little amount (less than 5%) of other two phases was observed.

The microstructure of the sample containing 6 %mol of Ta_2O_5 is presented in Fig. 1.

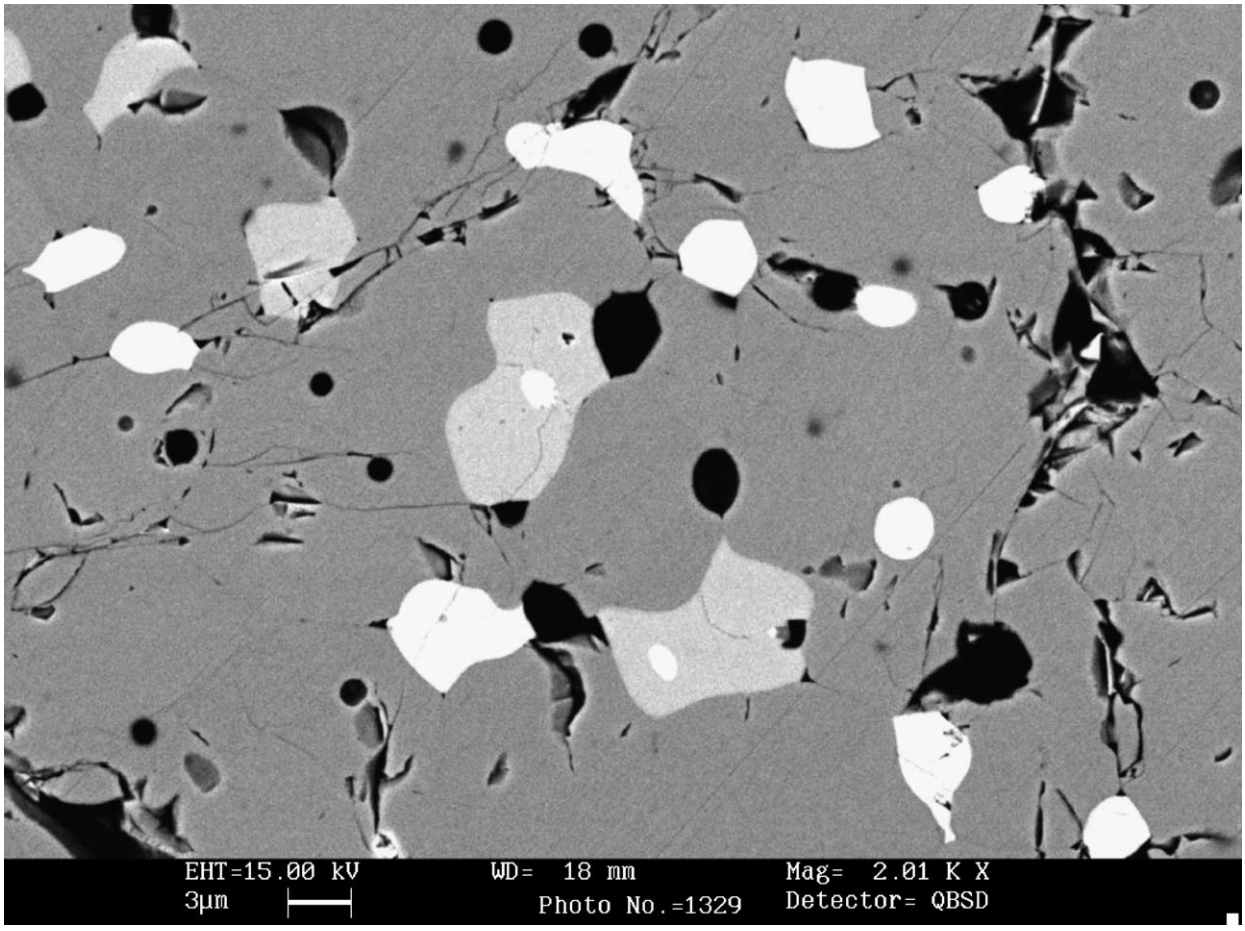

Fig. 1. SEM image showing the microstructure of the sample containing 6 %mol of Ta_2O_5. Two different phases dispersed in the matrix are clearly shown.

It is possible to see two different phases dispersed in the solid solution matrix. The chemical analysis performed with the EDS device allowed to establish that the brighter phase has a $2CeO_2$–Ta_2O_5 binary composition, whereas the grey inclusions containing also zirconia have a ZrO_2–$2CeO_2$–Ta_2O_5 ternary composition. However, the scarce accuracy of this analytical method did not allow to establish the exact chemical composition of the above mentioned phases, only later, with the help of the Rietveld method, the brighter phase was unambiguously identified to be the monoclinic compound $CeTaO_4$.

3.2. Analysis of the X-ray diffraction patterns

The presence of the two phases in the specimens containing 5 and 6% in Ta_2O_5 is confirmed also by the examination of the X-ray diffraction patterns. They show also some additional peaks attributable at these new crystalline phases (see later).

4. X-ray crystallographic study

4.1. Methods and programs used

Since the samples are nearly cubic, the usual visual analysis of the X-ray spectra might lead to an ambiguous determination of the crystal structure of the samples, on the contrary the Rietveld method is able to establish unambiguously, from the XRD spectra, the true structure of the various specimens and to provide information on particle size and instrumental broadening. The programs used were DBWS-9411 and DBWS-9807 for PC[29] and all the definition and interpretations of the numerical criteria of fit (R_p, R_{wp}, R_B, R_F, S = G.O.F.) were taken from these programs or from Table 1.3 – some often-used numerical criteria of fit – contained in the book of reference.[30] Other programs used were: DMPLOT[31] for performing the plot of the calculated and experimental XRD spectra presented in Figs. 2–10.

The atomic scattering factors of the ionic species, Zr^{4+}, Hf^{4+}, Ce^{4+}, Ta^{5+} were approximated using the coefficients reported on the International Tables for X-Ray Crystallography,[32] while the coefficients of O^{2-} where taken from reference.[33]

4.2. Parameters used in the Rietveld refinements

The Rietveld refinement carried out in the space group $Fm\bar{3}m$ presents 18 parameters that are: 1: one total scale factor; 2–7: six background parameters; 8–10: U, V, W half-width parameters entering in the parabolic formula of Cagliotti et al.;[34] 11: the cubic cell translation a; 12: the Rietveld asymmetry parameter applied to Bragg-peaks with $2\theta < 90^\circ$; 13–14: two parameters η_0 and η_t used for modelling the variation of the mixing parameter η with 2θ as $\eta = \eta_0 + \eta_t 2\theta$, η enter in the pseudo-Voigt (pV) function:

$$\mathrm{pV} = \eta L + (1 - \eta)G \quad (2)$$

where L is Lorentian function and G is Gaussian function; 15: one isotropic parameter U constrained to be equal for all the M^{n+} ions; 16: one isotropic parameter B for O^{2-} ion; 17:

Table 1
Rietveld refinement of specimen 1, $Ce_{0.60000}Zr_{0.39216}Hf_{0.00784}O_2$

Age in months	8	8	51	51
Crystal system	Cubic	Tetragonal	Cubic	Tetragonal
Space group	$Fm\bar{3}m$	$P4_2/nmc$	$Fm\bar{3}m$	$P4_2/nmc$
$a = b$ (Å)	5.3044(0)	3.7485(1)	5.3044(1)	3.7485(1)
c (Å)	–	5.3109(1)	–	5.3104(2)
Tetragonality (T)[a]	–	1.00183(2)	–	1.00174(2)
$c - a\sqrt{2}$	–	0.00972(2)	–	0.00922(3)
$U \times 10^3$ [$^\circ(2\vartheta)^2$]	122(4)	79(4)	138(7)	118(7)
$V \times 10^3$ [$^\circ(2\vartheta)^2$]	−23(4)	−14(3)	−17(6)	−25(6)
$W \times 10^3$ [$^\circ(2\vartheta)^2$]	11.7(8)	10.7(6)	1.3(1.1)	4.3(1)
η_0	0.68(1)	0.69(1)	0.91(2)	0.96(2)
η_t	0.0003(2)	0.0012(3)	−0.024(4)	−0.0024(4)
Asymmetry parameter	0.060(2)	0.057(2)	0.040(8)	0.037(8)
t(Sparks)	–	–	−0.18(8)	−0.14(9)
$B_{(Ce^{4+},Zr^{4+},Hf^{4+})}$	0.32(1)	0.32(1)	0.41(16)	0.33(16)
$Z_{(O^{2-})}$	0.5000	0.4811(13)	0.5000	0.4831(35)
$Z_{(O^{2-})}$ from T	–	0.4855	–	0.4859
$B_{(O^{2-})}$	1.74(6)	1.49(7)	1.47(18)	1.28(21)
Parameters number	18	20	19	21
R_B	2.45	2.44	3.80	3.78
R_F	1.63	2.02	2.30	2.84
R_p	9.02	8.61	9.72	9.53
R_{wp}	12.10	11.53	12.75	12.38
S = G.O.F.	1.72	1.64	1.16	1.13

[a] $T = c_t/(a_t\sqrt{2})$.

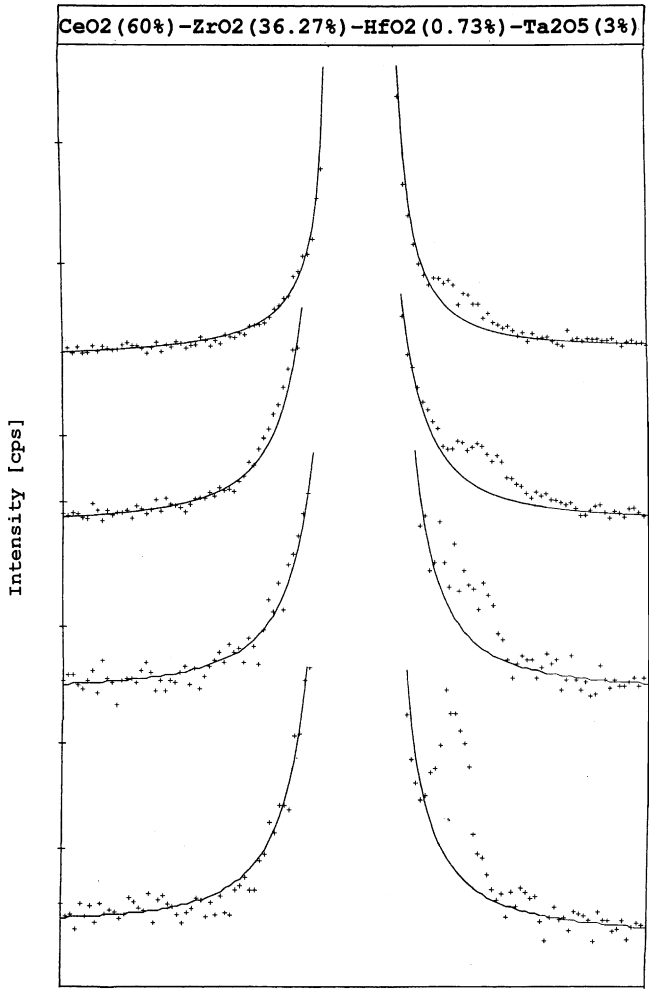

Fig. 2. Rietveld refinement plot of the Cu Kα data for specimen no. 4: [CeO_2 (60.00%)–ZrO_2 (36.27%)–HfO_2 (0.73%)–Ta_2O_5 (3.00%)], collected few days (≅10 days) after the sintering process. Note on the lower spectrum the small spurious peak on the right of the strong $(0\,1\,1)_t$ peak. The other spectra collected during 4 months after the sintering process show that this spurious peak is greatly reduced.

the G_1 March–Dollase parameter for modelling the preferred orientation;[35] 18: 2θ-zero point offset; and when needed 19: the *t* parameter of the Sparks et al.[36] model for surface roughness. Since the Rietveld refinement in the tetragonal space group $P4_2/nmc$ was always carried out with isotropic thermal parameters, only two new variables must be added and precisely the cell parameter c and the *z* coordinate of the O^{2-} ion.

5. Detailed analysis of the X-ray diffraction data

5.1. Specimen no. 1: $Ce_{0.60000}Zr_{0.39216}Hf_{0.00784}O_2$

The data collected after few days show only spurious peak of types A and B and the data are the same as those collected afterwards.

5.1.1. Rietveld refinement of the data collected after 8 months

The Rietveld refinement started in the space group $Fm\bar{3}m$ and presents 18 total parameters as explained in general discussion. The splitting of the peak in the 2θ regions at 70–72°, 78–79° and 80–82° is not so clear (see Fig. 10) to indicate a tetragonal specimen as it was found by Yashima et al.[12] for an analogous specimen but having composition $Ce_{0.65}Zr_{0.35}O_2$ (see Fig. 1 p. 1068 of Ref. [12]). Moreover, the $(0\,1\,2)_t$ peak at $2\theta = 41.65°$, is very weak but visible (see Fig. 10), so a second Rietveld refinement was carried out in the tetragonal space group $P4_2/nmc$, now two new variables must be added and precisely the cell parameter *c* and the *z* coordinate of the O^{2-} ion. Selected final parameters and *R* factors are reported in Table 1. It is evident that the refinement with the tetragonal space group gives *R* factors that are lower than the cubic ones, ΔR_{wp} = 12.10–11.53 = 0.57 and $R = R_{wp}(\text{cubic})/R_{wp}(\text{tetragonal}) = 1.0494$. Although the Hamilton test[37] suggest the tetragonal space group as more probable, we cannot use it because such significance test is not reliable in presence of heavy atoms.[38] However, taking also into account that the peak $(0\,1\,2)_t$ is effectively present, we have no doubt that this specimen is really tetragonal.

The very low *R* Bragg indices and the relatively high R_p and R_{wp} indices of the preceding refinements have prompted us to make a refinement with two phases for modelling better the profile fitting, for example two cubic phases or one cubic and one tetragonal or two tetragonal phase. Each phase is described by an appropriate pseudo-Voigt function. This is exactly equal to consider that the crystalline specimens possess a bimodal distribution as reported by Young and Sakthivel.[39]

The refinement with two phases have lowered significantly the R_p and R_{wp} factors especially for the tetragonal– tetragonal case (see Table 2). Tetragonality remains always very near to 1.00 or rather slightly lower than 1.00, so it is difficult to decide, using only tetragonality, if this specimen is tetragonal or cubic. Furthermore, we can say that this specimen is truly tetragonal on the basis of the Rietveld refinements and the presence of the tetragonal $(0\,1\,2)_t$ peak. Moreover, the presence of the $(0\,1\,2)_t$ peak and the tetragonality very near to 1.00 suggest that this specimen is a t'' phase.

5.1.2. Rietveld refinement of the data collected after 51 months

The Rietveld refinements, carried out on this specimen with the same modalities as the preceding ones, have shown that it preserves the tetragonal rather than the cubic structure (see Tables 1 and 2), also if the $(0\,1\,2)_t$ peak disappears almost completely (see Fig. 10), so we may classify it as a t' form.

5.1.3. Note on the tetragonality of the first specimen

Specimen no. 1 refines, both with data collected after 8 and 51 months, with a tetragonality lower than 1.00 that is a very unexpected result not easily explicable (see the discussion on tetragonality). However, in Tables 1 and 2 we report only the

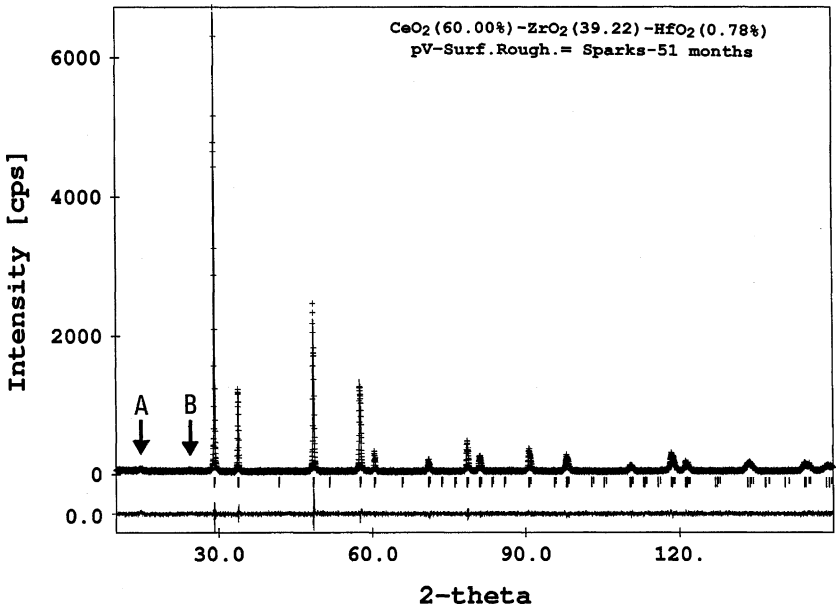

Fig. 3. Rietveld refinement plot of the Cu Kα data for specimen no. 1: [CeO_2 (60.00%)–ZrO_2 (39.22%)–HfO_2 (0.78%)], collected 51 months after the sintering process. The observed data are indicated by plus signs, the calculated profile is the continuous line overlaying them, and the lower curve is the difference between the observed and calculated intensity at each step. The row of vertical tick marks gives the position of all Bragg reflections. The additional weaker sharp peaks are distinguishable because they are without the vertical tick mark. In this manner two additional very weak sharp peaks (A and B) are distinguishable, they have fractional indices (1/2 0 1/2) and (1/2 1/2 1), respectively.

refinements with tetragonality greater than 1.00 also if they present *R* factors slightly greater. Moreover, this compound is very strange because it has been studied many times but it has been reported with different crystal structure depending on many factors as the particular chemical history, the sintering temperature, the quenching rate, the oxygen vacancies and so on. In fact, Meriani and coworkers[2–4] found for this composition a cubic phase with $a = 5.3049$ Å and a tetragonal t' phase with $a = 3.7315$ Å, $c = 5.3074$ Å, with tetragonality $T = 1.0057$, again Meriani and coworkers[7] found a cubic phase for a specimen sintered at 1600 °C for 2 h, and Yashima et al.[8,9] found a tetragonal t' phase with tetragonality $T = 1.005$ or a cubic one with $a = 5.3125$ Å. Finally Zhou[40] reported a fully stabilized cubic phase.

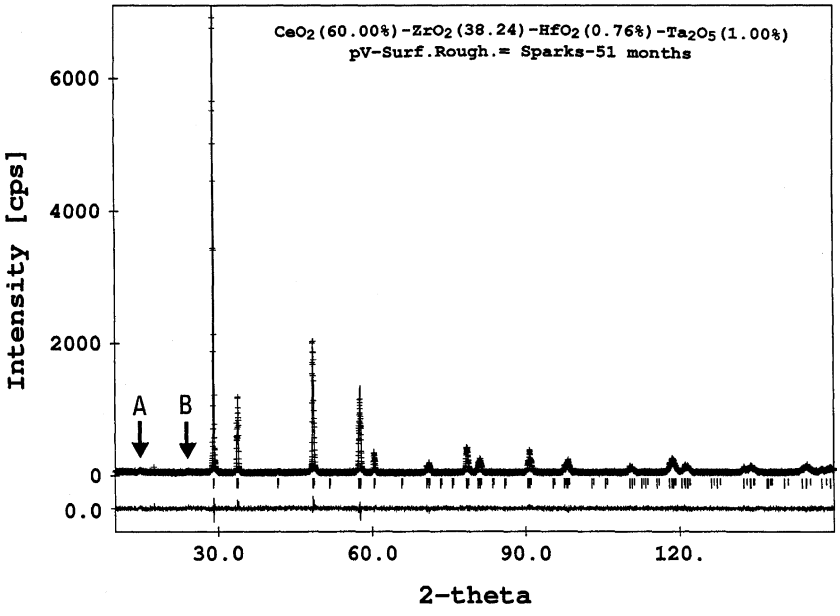

Fig. 4. Rietveld refinement plot of the Cu Kα data for specimen no. 2: [CeO_2 (60.00%)–ZrO_2 (38.24%)–HfO_2 (0.76%)–Ta_2O_5 (1.00%)], collected 51 months after the sintering process. Data presented as Fig. 3.

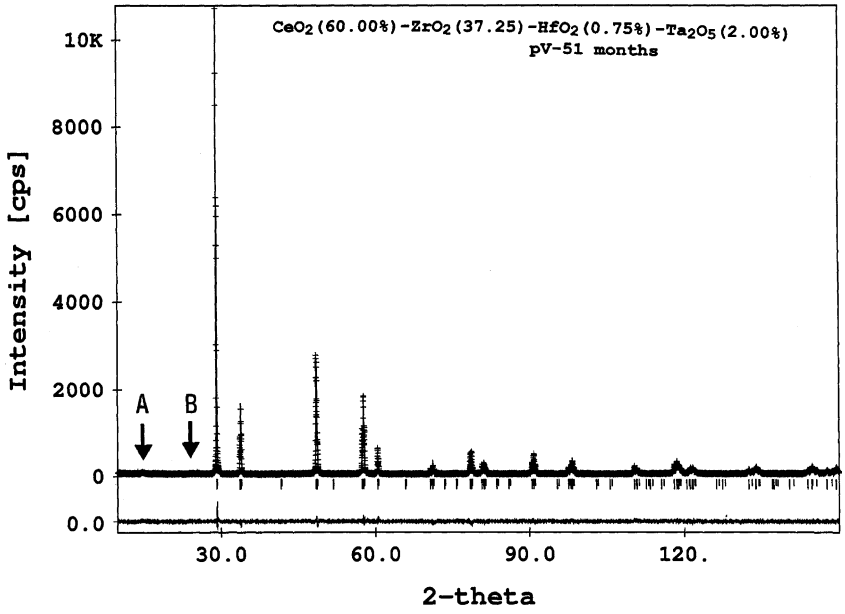

Fig. 5. Rietveld refinement plot of the Cu Kα data for specimen no. 3: [CeO_2 (60.00%)–ZrO_2 (37.25%)–HfO_2 (0.75%)–Ta_2O_5 (2.00%)], collected 51 months after the sintering process. Data presented as Fig. 3.

5.2. *Specimens containing Ta_2O from 1 to 6 mol%*

These specimens were refined either as cubic in space group $Fm\bar{3}m$ and as tetragonal in space group $P4_2/nmc$. This refinement was carried out using only the three parameters *U*, *V*, *W* for modelling peaks width while for modelling the profile shape the pseudo-Voigt function was used. The R_p and R_{wp} factors in the cubic system remained always very high but more important the calculated spectrum did not fit with the experimental data. When the tetragonal space group $P4_2/nmc$ was used a better agreement was obtained. All the specimens containing Ta_2O_5 are tetragonal with space group $P4_2/nmc$ (No. 137), however the tetragonality of the six specimens (see Tables 3a and 3b) is very near to 1.00, i.e. they are nearly cubic. The difference $c - a\sqrt{2}$, although very little, being in the range 0.0208(4)–0.03494(8) Å, is surely significant for the high reliability of the lattice constants determined by using the Rietveld method.

As already reported, the specimens no. 6 (5% in Ta_2O_5) and 7 (6% in Ta_2O_5) are formed by three phases, the most important is the usual tetragonal phase but a little amount (less than 5%) formed by other two phases is present. We

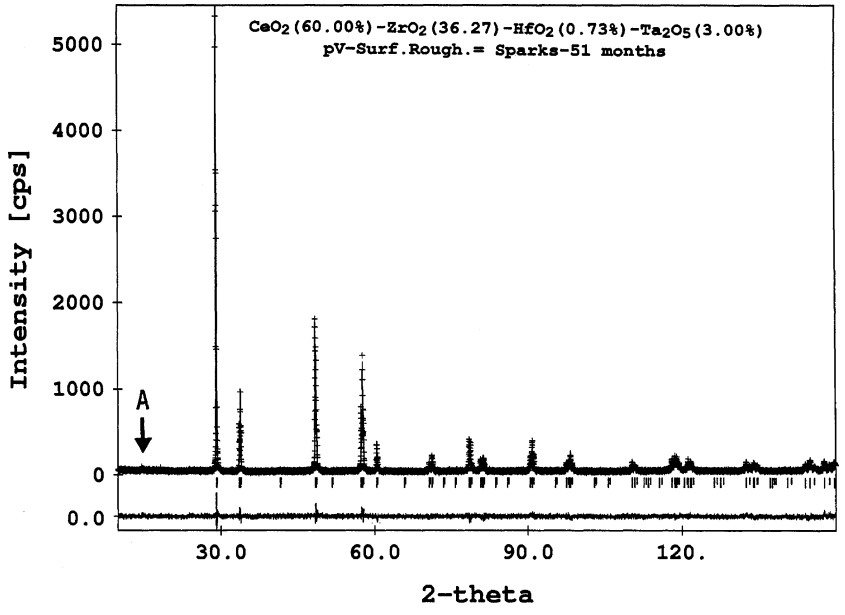

Fig. 6. Rietveld refinement plot of the Cu Kα data for specimen no. 4: [CeO_2 (60.00%)–ZrO_2 (36.27%)–HfO_2 (0.73%)–Ta_2O_5 (3.00%)], collected 51 months after the sintering process. Only one additional peak (A) with fractional indices (1/2 0 1/2) is present, other data as Fig. 3.

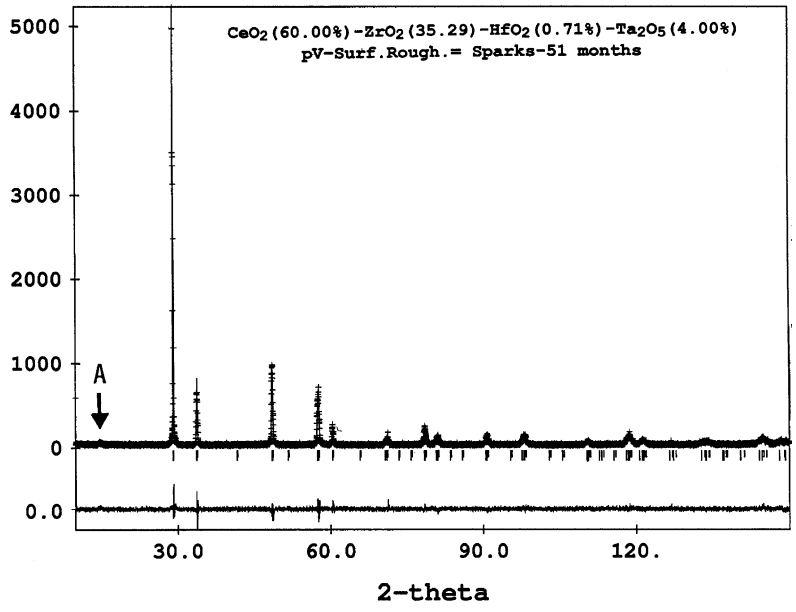

Fig. 7. Rietveld refinement plot of the Cu Kα data for specimen no. 5: [CeO_2 (60.00%)–ZrO_2 (35.29%)–HfO_2 (0.71%)–Ta_2O_5 (4.00%)], collected 51 months after the sintering process. Only one additional peak (A) with fractional indices (1/2 0 1/2) is present, other data presented as Fig. 3.

have ascertained that one phase is surely constituted by the monoclinic compound cerium tantalum oxide ($CeTaO_4$). The crystal and molecular structure of this compound is well know[41] (monoclinic, space group $P2_1/c$ (No. 14)) because it has been refined with the Rietveld method using neutron powder diffraction data. Thus, several least-squares cycles were carried out handling two phases simultaneously, while the third phase, that is present in very small amount, was not considered. The final results are reported in Tables 3a and 3b.

During some Rietveld refinements very low or also negative thermal factors were found for metal atoms while that of the O^{2-} anion was nearly zero, this will be explained later under the section on microabsorption.

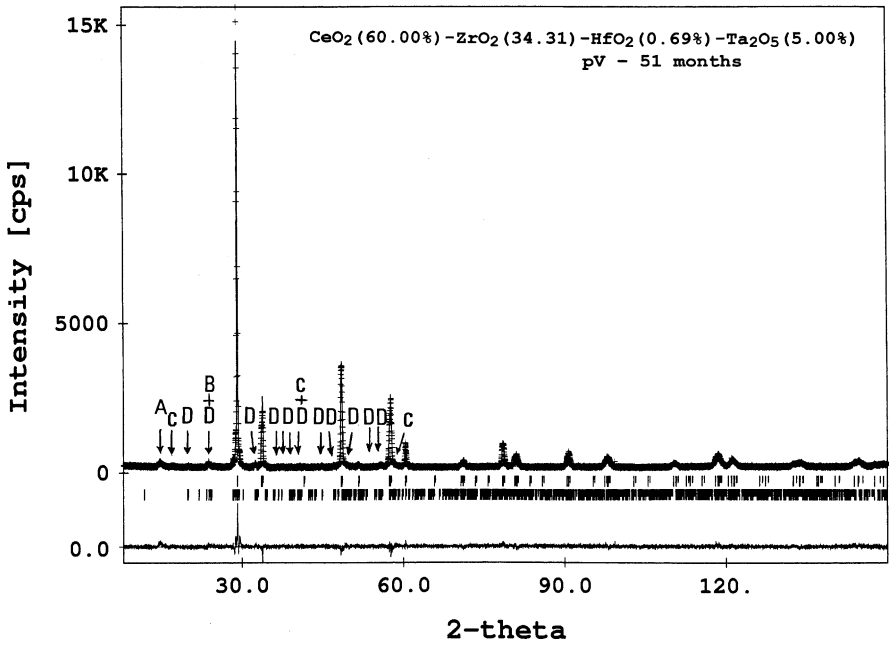

Fig. 8. Rietveld refinement plot of the Cu Kα data for specimen no. 6: [CeO_2 (60.00%)–ZrO_2 (34.31%)–HfO_2 (0.69%)–Ta_2O_5 (5.00%)], collected 51 months after the sintering process. Spurious peaks A and B have indices (1/2 0 1/2) and (1/2 1/2 1), respectively. Now is also present, for the first time, a second row of vertical tick marks, it gives the position of the Bragg reflections due to the monoclinic compound $CeTaO_4$. Since these peaks are very weak and the tick marks are very crowded, we have indicated for clarity the strongest of these peaks with the letter D. Peaks of type C are due to the third phase with composition ZrO_2–$2CeO_2$–Ta_2O_5. Other data presented as Fig. 3.

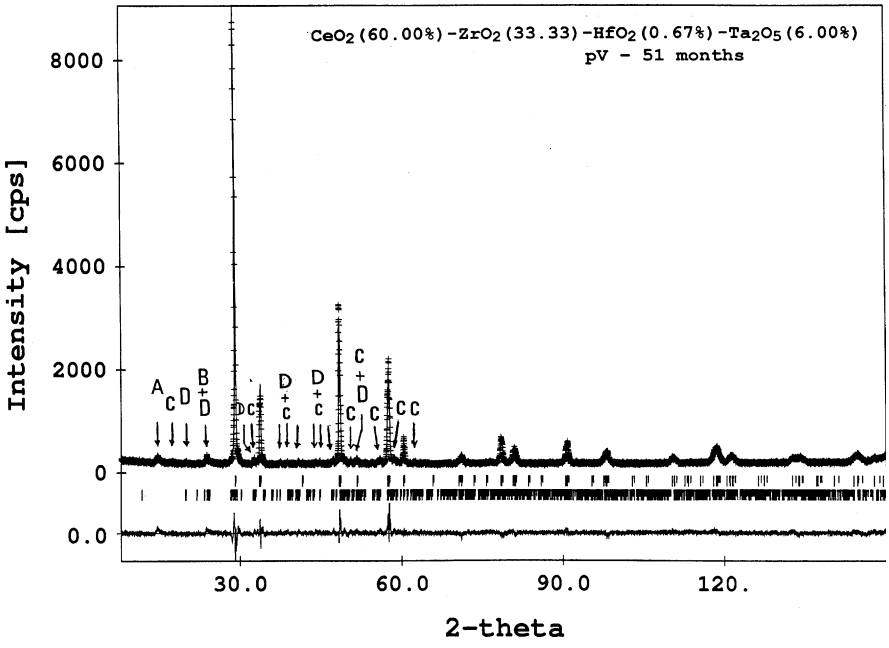

Fig. 9. Rietveld refinement plot of the Cu Kα data for specimen no. 7: [CeO_2 (60.00%)–ZrO_2 (33.33%)–HfO_2 (0.67%)–Ta_2O_5 (6.00%)], collected 51 months after the sintering process. Peaks of types A, B, C and D have the same meaning as in Fig. 8. Other data as Fig. 3.

5.2.1. Additional very weak sharp peaks

The XRD spectra of the specimens having molecular composition 1, 2, 3, and 4% in Ta_2O_5, especially when the specimens are freshly prepared, show additional very weak sharp peaks that cannot be indexed in terms of a simple unit cell. These spurious peaks can be separated in two types, those that can be indexed using a tetragonal supercell with A = B = 2*a* = 2*b*, C = 2*c*, and those that cannot be indexed with this or any other supercell. The first type includes only two peaks, identified in the figures with the letter A or B, while the second type includes several reflections, overall identified with the label C. One or two evident peaks of C type

Table 2
Rietveld refinement of specimen 1, $Ce_{0.60000}Zr_{0.39216}Hf_{0.00784}O_2$ using bimodal distribution

Age in months			8			51
Number of phases			2			2
Crystal system	Tetragonal		Tetragonal	Tetragonal		Tetragonal
Space group	$P4_2/nmc$		$P4_2/nmc$	$P4_2/nmc$		$P4_2/nmc$
$a = b$ (Å)	3.74503(9)		3.75012(4)	3.7444(2)		3.7505(1)
c (Å)	5.31046(19)		5.31002(9)	5.3157(2)		5.3096(2)
Tetragonality (T)[a]	1.00268(21)		1.00124(10)	1.0038(3)		1.0011(3)
$c - a\sqrt{2}$	0.01419(22)		0.00655(10)	0.02032(3)		0.00559(3)
$U \times 10^3$ [°$(2\vartheta)^2$]	106(11)		22(1)	66(12)		47(6)
$V \times 10^3$ [°$(2\vartheta)^2$]	−38(8)		−51(3)	6(9)		−3(5)
$W \times 10^3$ [°$(2\vartheta)^2$]	9(1)		46(2)	0.10(19)		1.7(9)
η_0	0.00(6)		0.20(1)	1.00(7)		0.64(8)
η_t	0.0083(7)		0.0139(3)	0.00(1)		0.0004(10)
Asymmetric parameter	0.059(9)		0.049(2)	0.058(9)		0.059(9)
t(Sparks)	–		–	−0.14(9)		−0.14(9)
$B_{(Ce^{4+},Zr^{4+},Hf^{4+})}$		0.35(2)			0.35(15)	
$Z_{(O^{2-})}$	0.4795(10)		0.4795(10)	0.4846(10)		0.4846(35)
$Z_{(O^{2-})}$ from T	0.4825		0.4881	0.4790		0.4890
$B_{(O^{2-})}$	1.36(6)		1.36(6)	1.29(20)		1.29(20)
Parameters number		28			28	
R_B (%)	2.06		2.20	4.07		2.98
R_F (%)	1.85		1.88	2.97		2.41
R_p		6.98			8.77	
R_{wp}		9.98			11.73	
S = G.O.F.		1.42			1.07	
Relative phase mass (%)	39.43		60.57	51.68		48.32

[a] Tetragonality (T) is defined as $T = c_t/(a_t\sqrt{2})$.

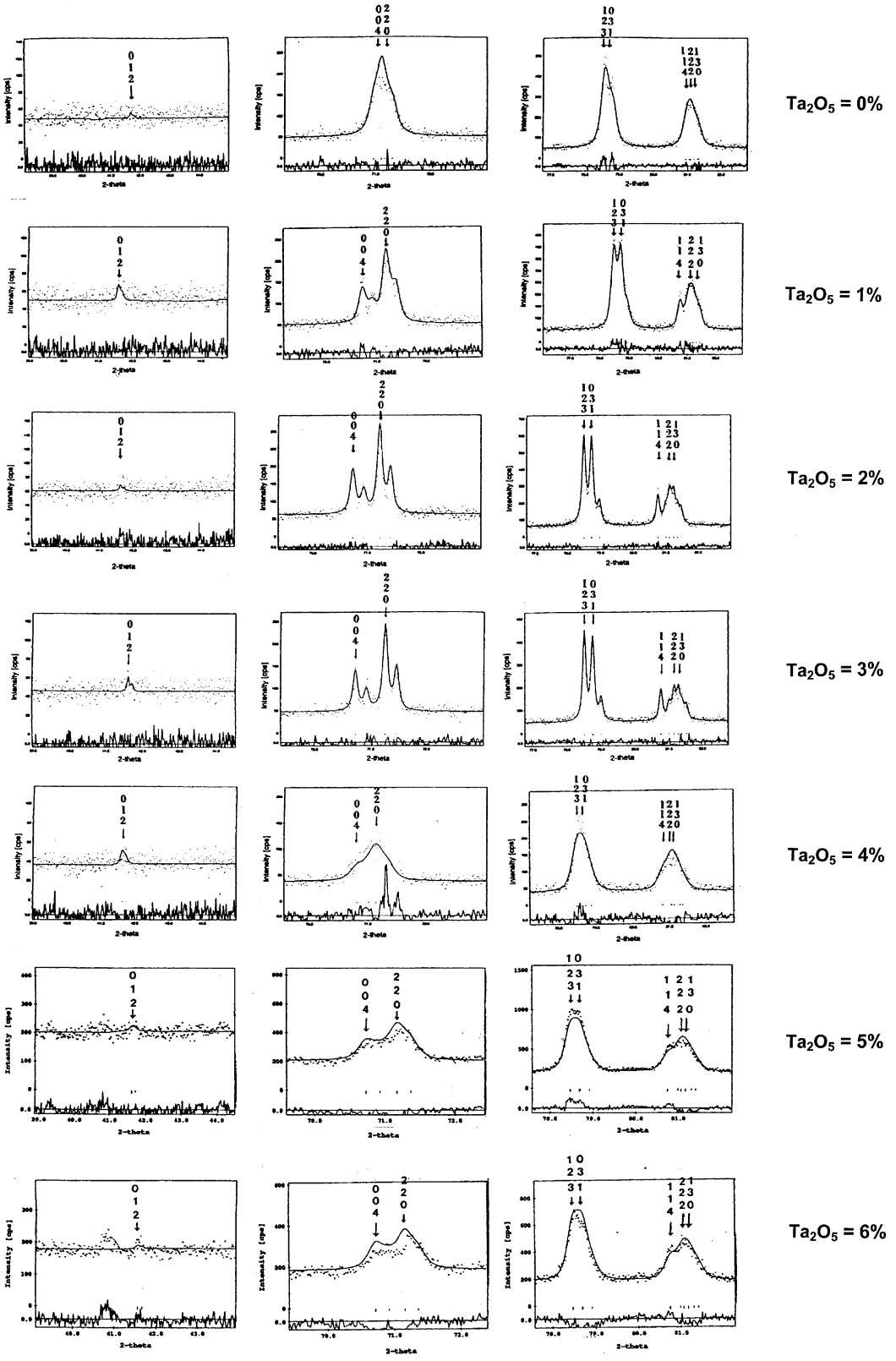

Fig. 10. This figure shows the peaks that better provide the tetragonal nature of the samples collected after 51 months (the samples collected after 8 months show a similar trend so they are not reported). The Miller indices are positioned upper the Cu Kα1 peak. The very weak $(0\,1\,2)_t$ peak is due only to the little displacement of the oxygen atom from its cubic position; the $(0\,0\,4)_c$ peak is splitted in $(0\,0\,4)_t$ + $(2\,2\,0)_t$ at 2θ region 70–72°; the $(1\,3\,3)_c$ peak is splitted in $(1\,2\,3)_t$ + $(0\,3\,1)_t$ at 2θ region 78–79°; and $(0\,2\,4)_c$ is splitted in $(1\,1\,4)_t$ + $(2\,2\,2)_t$ + $(1\,3\,0)_t$ at 2θ region 80–82°. The splitting increases as the Ta_2O_5 content increases, reaching a maximum for Ta_2O_5 = 3% where the Kα1 and Kα2 peaks are clearly visible, but starting with Ta_2O_5 = 4% the peak overlap increases and the splitting is less evident.

Table 3a
Rietveld refinement of specimens with variable Ta_2O_5 content, collected after 8 months

Specimen number	2	3	4	5	6	7
Ta_2O_5 content (%)	1	2	3	4	5	6
Crystal system	Tetragonal	Tetragonal	Tetragonal	Tetragonal	Tetragonal	Tetragonal
Space group	$P4_2/nmc$	$P4_2/nmc$	$P4_2/nmc$	$P4_2/nmc$	$P4_2/nmc$	$P4_2/nmc$
$a = b$ (Å)	3.74527(5)	3.74498(4)	3.74281(3)	3.74585(1)	3.74357(1)	3.74150(8)
c (Å)	5.32709(9)	5.32842(7)	5.32768(6)	5.3182(3)	5.32601(10)	5.32496(14)
Tetragonality (T)[a]	1.00575(10)	1.00608(9)	1.00653(8)	1.0039(4)	1.00601(14)	1.00636(16)
$c - a\sqrt{2}$	0.03048(10)	0.03222(8)	0.03455(7)	0.0208(4)	0.03180(12)	0.03368(16)
$U \times 10^3$ [°$(2\vartheta)^2$]	59(3)	20(2)	9(1)	167(1)	68(5)	52(4)
$V \times 10^3$ [°$(2\vartheta)^2$]	−10(3)	−6(2)	5(1)	9(1)	11(2)	19(5)
$W \times 10^3$ [°$(2\vartheta)^2$]	17.5(9)	11.4(6)	5.3(4)	−9.6(3)	5(1)	5.0(1)
η_0	0.41(1)	0.51(2)	0.70(2)	0.90(4)	0.63(2)	0.80(2)
η_t	0.0027(3)	0.0036(4)	0.027(4)	0.000(5)	0.000(5)	0.000(8)
Asymmetry parameter	0.090(4)	0.077(6)	0.082(6)	0.043(15)	0.000(6)	0.000(6)
t(Sparks)	−0.46(2)	−0.25(4)	–	–	–	–
$B_{(Ce^{4+},Zr^{4+},Hf^{4+})}$	0.66(7)	0.40(2)	0.54(1)	0.62(4)	0.43(2)	0.54(2)
$Z_{(O^{2-})}$	0.4735(6)	0.4788(16)	0.4747(13)	0.4663(4)	0.5358(21)	0.5227(32)
$Z_{(O^{2-})}$ from T	0.4744	0.4736	0.4727	0.4786	0.5262	0.5269
$B_{(O^{2-})}$	1.90(9)	2.13(9)	0.76(9)	4.02(33)	1.41(11)	2.40(16)
Number of parameters	21	21	20	20	20	20
R_B (%)	4.28	7.99	7.90	7.23	6.09	5.24
R_F (%)	3.28	6.20	6.36	4.90	5.09	3.98
R_p (%)	9.15	11.92	11.36	12.46	7.76	8.26
R_{wp} (%)	12.80	15.18	14.49	16.28	10.15	11.61
S = G.O.F.	1.52	1.90	1.95	1.25	1.60	1.86

[a] Tetragonality (T) is defined as $T = c_t/(a_t\sqrt{2})$.

Table 3b
Rietveld refinement of specimens with variable Ta_2O_5 content, collected after 51 months

Specimen number	2	3	4	5	6	7
Ta_2O_5 content (%)	1	2	3	4	5	6
Crystal system	Tetragonal	Tetragonal	Tetragonal	Tetragonal	Tetragonal	Tetragonal
Space group	$P4_2/nmc$	$P4_2/nmc$	$P4_2/nmc$	$P4_2/nmc$	$P4_2/nmc$	$P4_2/nmc$
$a = b$ (Å)	3.74461(6)	3.74394(3)	3.74099(4)	3.7462(1)	3.74519(8)	3.74317(11)
c (Å)	5.32673(11)	5.32700(5)	5.32550(7)	5.3190(3)	5.32547(18)	5.32253(23)
Tetragonality (T)[a]	1.00586(13)	1.00609(8)	1.00660(9)	1.0040(4)	1.00547(20)	1.00546(26)
$c - a\sqrt{2}$	0.03105(13)	0.03227(6)	0.03494(8)	0.0211(4)	0.02897(19)	0.02889(26)
$U \times 10^3$ [°$(2\vartheta)^2$]	65(4)	16(1)	13(9)	17(2)	90(8)	246(16)
$V \times 10^3$ [°$(2\vartheta)^2$]	−3(4)	6(1)	4(2)	7(17)	50(8)	−116(14)
$W \times 10^3$ [°$(2\vartheta)^2$]	3.5(7)	0.5(2)	1.7(3)	−9(3)	−5(2)	32(3)
η_0	0.64(2)	0.78(2)	0.92(2)	0.90(4)	0.70(2)	0.71(2)
η_t	0.0016(4)	0.0020(3)	0.0002(3)	0.000(8)	0.000(8)	0.000(9)
Asymmetry parameter	0.033(10)	0.00(1)	0.026(20)	0.045(16)	0.012(7)	0.010(7)
t(Sparks)	−0.26(6)	–	−0.50(2)	–	–	–
$B_{(Ce^{4+},Zr^{4+},Hf^{4+},Ta^{5+})}$	0.72(13)	0.39(1)	1.52(11)	0.62(36)	0.69(2)	0.27(3)
$Z_{(O^{2-})}$	0.4721(14)	0.4836(30)	0.4715(12)	0.4565(34)	0.5432(22)	0.5328(31)
$Z_{(O^{2-})}$ from T	0.4741	0.4736	0.4726	0.4787	0.5250	0.5250
$B_{(O^{2-})}$	1.48(16)	1.95(11)	2.51(15)	3.53(32)	3.65(20)	1.77(20)
Number of parameters	20	19	20	19	20	20
R_B (%)	4.16	5.19	8.34	8.11	7.20	7.63
R_F (%)	3.01	4.38	6.31	5.33	3.61	5.44
R_p (%)	8.88	8.45	10.47	12.65	6.86	7.59
R_{wp} (%)	11.60	11.12	13.48	16.44	9.11	10.00
S = G.O.F.	1.07	1.12	1.16	1.26	1.54	1.57

[a] $T = c_t/(a_t\sqrt{2})$.

are often found in opposite side of the strongest reflections: $(0\,1\,1)_t$, $(0\,0\,2)_t$–$(1\,1\,0)_t$, $(1\,1\,2)_t$–$(0\,2\,0)_t$ and $(0\,1\,3)_t$–$(1\,2\,1)_t$, as an example Fig. 2 reports the small spurious peak on the right of the strong $(0\,1\,1)_t$ peak for the freshly prepared specimen containing 3 mol% in Ta_2O_5. Fig. 2 also shows the evolution of this spurious peak in nearly 4 months, its intensity is greatly reduced.

In fact for the compounds having molecular composition 1, 2, 3, and 4% in Ta_2O_5 these weak additional peaks of type C completely disappear after 8 months. A and B peaks are greatly reduced with time but they are still evident after 51 months, only B peak disappear completely for the specimens having composition 3 and 4% (see Figs. 6 and 7). However, we wish to remark that such additional peaks are very weak.

A possible explanation of these very weak extra-peaks is the formation of a new phase during the sintering process, but a detailed search has not revealed such a new phase. A more reasonable explanation arises by considering that in the CeO_2–ZrO_2 system there are usually a 2–3% in vacancies of oxygen atoms, then the usage as dopant of Ta_2O_5, that possesses an half oxygen atom more than CeO_2 or ZrO_2, eliminates these vacancies as far as the 3% is reached. When the composition in Ta_2O_5 exceeds 3% vacancies in metal atoms arise, producing disorder or also density modulation. The presence of modulated structures has been already reported for anion-excess zirconia–niobia alloys.[42]

For this reasons we have carried out Rietveld refinements using specimens 8 months or even 51 months old, in this manner we are sure that the presence of disorder and modulation is greatly reduced. However, refinements using the freshly prepared specimens confirm that the basic structure of these samples is tetragonal, although the *R* factors are higher than usual.

When the molecular composition in Ta_2O_5 is 5 or 6%, the number and the intensity of these spurious peaks increases, they are identified in Figs. 8 and 9 with the label C or D and they do not disappear with time. As already explained these extra peaks are due to the presence of a little amount of $CeTaO_4$ and of a third phase having a ZrO_2–$2CeO_2$–Ta_2O_5 ternary composition.

5.2.2. Microabsorption

During the refinement of the specimen no. 2 and 3 collected after 8 months and specimen no. 1, 2, and 4 collected after 51 months, the isotropic thermal factors of the M^{n+} cations became very low or also strongly negative ($B \cong -0.50$), while that of O^{2-} anion was nearly zero. This effect has been attributed by several authors to microabsorption (bulk porosity and surface roughness)[36,43,44] that decreases systematically the intensities of the sample in the low angle region then, during the refinement, the thermal factors become very low or also negative in order to increase the structure factor F_h at low 2θ.

In these cases, the refinement was continued introducing the microabsorption model of Sparks et al.[36] in which the intensities are multiplied by a function $S_R(\theta)$ given by:

$$S_R(\theta) = 1.00 - t\left(\theta - \frac{\pi}{2}\right) \tag{3}$$

that must be equal to 1.00 when the diffracted X-ray is backscattered. With this model only one new parameter (t) must be introduced in the refinement and it is reported, when needed, in Tables 1, 2, 3a and 3b together with the other parameters. Other microabsorption models are available but in the present cases they did not give satisfactory results.

6. Size-strain broadening analysis of the seven specimens

These seven specimens present peaks broadened at a different degree, the less broadened is the sample no. 4. Then, for clarifying this point we have attempted a Rietveld refinement with the Thompson–Cox–Hastings pseudo-Voigt profile function[45] modified by Young and Desai[46] (code NPROF = 7 in program DBWS-9411 and DBWS-98). In this manner the full-width-at-half-maximum (Γ) can be divided in two components one gaussian (Γ_g) and the other lorentian component (Γ_l) as reported below:

$$\Gamma_g = \left(U\tan^2\theta + V\tan\theta + W + \frac{Z}{\cos^2\theta}\right)^{1/2} \tag{4}$$

and

$$\Gamma_l = X\tan\theta + \frac{Y}{\cos\theta} \tag{5}$$

from these relations one can see that microstrain broadening has two components, one lorentian ($X\tan\theta$) and the other one gaussian ($\Delta U^{1/2}\tan\theta$) (while usually the microstrain broadening is taken to be only gaussian[47]). Also the size broadening has two components, one lorentian ($Y/\cos\theta$) and the other gaussian ($Z^{1/2}/\cos\theta$) (while usually the size broadening is taken to be only lorentian[47]). In order to have information on these quantities we have followed the *weighted method* of Paiva-Santos et al.[48] and we give here the complete explicit formulas for the weighted crystallite size p (Å) and for the rms microstrain $\langle\varepsilon\rangle$ because they are not reported elsewhere:

$$p\,(\text{Å}) = \frac{k\,\lambda 180^\circ}{[(\sqrt{Z})^5 + A(\sqrt{Z})^4(\Delta Y) + B(\sqrt{Z})^3(\Delta Y)^2 + C(\sqrt{Z})^2(\Delta Y)^3 + D(\sqrt{Z})(\Delta Y)^4 + (\Delta Y)^5]^{1/5}\pi} \tag{6}$$

$$\text{the r.m.s. microstrain } \langle\varepsilon\rangle = \frac{\Delta d}{d} = -\frac{\Delta d^*}{d^*}:$$

$$(\varepsilon) = \frac{[(\sqrt{\Delta U})^5 + A(\sqrt{\Delta U})^4(\Delta X) + B(\sqrt{\Delta U})^3(\Delta X)^2 + C(\sqrt{\Delta U})^2(\Delta X)^3 + D(\sqrt{\Delta U})(\Delta X)^4 + (\Delta X)^5]^{1/5}\pi}{K_d 180^\circ} \tag{7}$$

Table 4
rms microstrains refined with the Paiva Santos "weighted method"[a]

Specimen number	1	1	2	2	3	3	4	4	5	5	6
Ta_2O_5 (%)	0	0	1	1	2	2	3	3	4	4	5
Age in months	8	51	8	51	8	51	8	51	8	51	8
Strain_$G \times 10^2$	0.114	0.049	0.135	0.120	0.044	0.000	0.000	0.000	0.100	0.123	0.018
Strain_$L \times 10^2$	0.074	0.138	0.029	0.081	0.019	0.065	0.029	0.060	0.110	0.105	0.163
Strain_WGT $\times 10^2$	0.159	0.154	0.150	0.168	0.054	0.065	0.029	0.060	0.140	0.188	0.166

[a] The composition 5% (51 months) and 6% (8 and 51 months) are not reported in this table because the Rietveld refinement, carried out using the method described in Section 6, was not successful because the FWHM of reflection $(0\,1\,1)_t$ became negative, probably for the presence of several additional peaks (see text).

where the symbols are exactly those used by Paiva-Santos et al.,[48] for example: k is the Scherrer constant taken to be 1, K_d was taken to be 2.00, $\Delta Y = Y_s - Y_i$, where Y_s is the Y parameter of the sample under study and Y_i that of the standard sample, $\Delta U = U_s - U_i$, where U_s is the U parameter of the sample under study and U_i that of the standard sample and so on. The parameters U_i, V_i, W_i, X_i, and Y_i were determined using the standard sample reported at the end of this work. From these results, shown in Table 4, at least some qualitative conclusions can be taken:

1. in all the specimens the broadening is due to microstrain while size broadening is practically absent. This means that the specimens are formed by great crystallites with very large size (>2000 Å), in accordance with the high sintering temperature;
2. the specimens collected after 8 months present a gaussian microstrain broadening that is always greater than the lorentian component (i.e. in accordance with the usual theory that microstrain broadening is principally gaussian). Two specimens collected after 51 months make exception to this rule;
3. the sample no. 4, $Ce_{0.58252}Zr_{0.35218}Hf_{0.00704}Ta_{0.05826}O_{2.02913}$, presents a weighted microstrain that is very low and this explains its particular behaviour;
4. the microstrain broadening seems to grow with time, in fact all the samples collected after 51 months show a little increment of microstrain broadening.

7. SiO_2 standard sample

In order to determine the U_i, V_i, W_i, X_i, and Y_i instrumental parameters we have performed a Rietveld refinement using the data collected on a standard SiO_2 specimen. This specimen exhibits an insignificant amount of intrinsic diffraction broadening.

Acknowledgments

We are very grateful to Prof. R.A. Young of the School of Physics, Georgia Institute of Technology, Atlanta (USA) for providing us the programs DBWS-9411, DBWS-9807 and DMPLOT. We are also indebted to Prof. C.O. Paiva-Santos of the Instituto de Quimica—UNESPD, Araraquara (Brazil) for valuable discussions and contributions in understanding the cristallite size and microstrains of these samples.

References

1. Meriani, S., A new single-phase tetragonal CeO_2–ZrO_2. *Mater. Sci. Eng.*, 1985, **71**, 369–373.
2. Meriani, S., Metastable tetragonal CeO_2–ZrO_2 solid solution. *J. de Physique (les V lis. Fr.)*, 1986, **47**(Suppl. 2), 485–489.
3. Meriani, S. and Spinolo, G., Powder data for metastable $Zr_xCe_{1-x}O_2$ (x = 0.84 to 0.40) solid solutions with tetragonal symmetry. *Powder Differ.*, 1987, **2**, 255–256.
4. Meriani, S., Features of the caeria-zirconia system. *Mater. Sci. Eng.*, 1989, **A109**, 121–130.
5. Yoshimura, M., Phase stability of zirconia. *Am. Ceram. Soc. Bull.*, 1988, **67**, 1950–1955.
6. Yashima, M. and Yoshimura, M., Thermodynamical models for phase changes between tetragonal and cubic phases in ZrO_2–CeO_2 solid solution. *Jpn. J. Appl. Phys.*, 1992, **31**, L1614–L1617.
7. Maschio, S., Sbaizero, O. and Meriani, S., Mechanical properties in the ceria-zirconia system. *J. Eur. Ceram. Soc.*, 1992, **9**, 127–132.
8. Yashima, M., Morimoto, K., Ishizawa, N. and Yoshimura, M., Zirconia-ceria solid solution synthesis and the temperature-time-transformation diagram for the 1:1 composition. *J. Am. Ceram. Soc.*, 1993, **76**, 1745–1750.
9. Yashima, M., Morimoto, K., Ishizawa, N. and Yoshimura, M., Diffusionless tetragonal-cubic transformation temperature in zirconia-ceria solid solutions. *J. Am. Ceram. Soc.*, 1993, **76**, 2865–2868.
10. Torng, S., Miyazawa, K. and Sakuma, T., Role of oxygen vacancies on cubic-tetragonal phase transition in ZrO_2–CeO_2. *Mater. Sci. Technol.*, 1995, **11**, 130–135.
11. Kim, D.-J. and Jung, H.-J., Raman spectroscopy of tetragonal zirconia solid solutions. *J. Am. Ceram. Soc.*, 1993, **76**, 2106–2108.
12. Yashima, M., Arashi, H., Kakihama, M. and Yoshimura, M., Raman scattering study of cubic-tetragonal phase transition in $Zr_{1-x}Ce_xO_2$ solid solution. *J. Am. Ceram. Soc.*, 1994, **77**, 1067–1071.
13. Yashima, M., Ohtake, K., Kakihana, M. and Yoshimura, M., Synthesis of metastable tetragonal (t') zirconia-ceria solid solutions by the polymerised complex method. *J. Am. Ceram. Soc.*, 1994, **77**, 2773–2776.
14. Yashima, M., Arashi, H., Kakihama, M. and Yoshimura, M., Raman scattering study of cubic-tetragonal phase transition in $Zr_{1-x}Ce_xO_2$ solid solution. *J. Am. Ceram. Soc.*, 1994, **77**, 1067–1071.
15. Duwez, P. and Odell, F., Phase relationships in the system zirconia-ceria. *J. Am. Ceram. Soc.*, 1950, **33**, 274–283.
16. Longo, V. and Roitti, S., Solid state phase relations in the system ZrO_2–CeO_2. *Ceramurgia Int.*, 1971, **1**, 4–10.
17. Roitti, S. and Longo, V., Investigation of phase equilibrium diagrams among oxides by means of electrical conductivity measurements. Application of the method to the system ZrO_2–CeO_2. *Ceramurgia Int.*, 1972, **2**, 97–102.

18. Tani, E., Yoshimura, M. and Sömiya, S., Revised phase diagram of the system ZrO_2–CeO_2 below 1400 °C. *J. Am. Ceram. Soc.*, 1983, **66**, 506–510.
19. Duran, P., Gonzales, M., Moure, C., Jurado, J. R. and Pascual, C., A new tentative phase equilibrium diagram for the ZrO_2–CeO_2 system in air. *J. Mater. Sci.*, 1990, **25.**, 5001–5006.
20. Yashima, M., Takashina, H., Kakihana, M. and Yoshimura, M., Low-temperature phase equilibria by the flux method and the metastable-stable phase diagram in the ZrO_2–CeO_2 system. *J. Am. Ceram. Soc.*, 1994, **77**, 1869–1874.
21. Yashima, M., Takashina, H., Kakihana, M. and Yoshimura, M., Assessment of the phase diagram in the ZrO_2–CeO_2 system. *Report of the Research Laboratory of Engineering Materials*, *Vol 19*. Tokio Institute of Technology, 1994 (pp. 41–50, and references therein).
22. Schomaker, V. and Marsh, R. E., Some comments on refinement in a space group of unnecessarily low symmetry. *Acta Cryst.*, 1979, **B35**, 1933–1934.
23. Howard, C. J. and Hunter, B. A., Oxygen position and bond lengths from lattice parameters in tetragonal zirconias. *J. Am. Ceram. Soc.*, 1998, **81**, 241–243.
24. Ranga Rao, M. G., Kašpar, J., Meriani, S., Di Monte, R. and Graziani, M., NO decomposition over partially reduced metallized CeO_2–ZrO_2 solid solutions. *Catal. Lett.*, 1994, **24**, 107–112.
25. Fornasiero, P., Di Monte, R., Ranga Rao, M. G., Kašpar, J., Meriani, S., Trovarelli, A. *et al.*, Rh-loaded CeO_2–ZrO_2 solid solutions as highly efficient oxygen exchangers: dependance of the reduction behaviour and the oxygen storage capacity on the structural properties. *J. Catal.*, 1995, **151**, 168–177.
26. Balducci, G., Fornasiero, P., Di Monte, R., Kašpar, J., Meriani, S. and Graziani, M., An unusual promotion of the redox behaviour of CeO_2–ZrO_2 solid solutions upon sintering at high temperatures. *Catal. Lett.*, 1995, **33**, 193–200.
27. Fornasiero, P., Balducci, G., Di Monte, R., Kašpar, J., Sergo, V., Gubitosa, G. *et al.*, Modification of the redox behaviour of CeO_2 induced by structural doping with ZrO_2. *J. Catal.*, 1996, **164**, 173–183.
28. Fornasiero, P., Kašpar, J., Sergo, V. and Graziani, M., Redox behavior of high-surface-area Rh-, Pt-, and Pd-loaded $Ce_{0.5}Zr_{0.5}O_2$ mixed oxide. *J. Catal.*, 1999, **182**, 56–69.
29. Young, R. A., Saktivel, A., Moss, T. S. and Paiva-Santos, C. O., DBWS-9411—an upgrade of the DBWS. Programs for Rietveld refinement with PC and mainframe computers. *J. Appl. Cryst.*, 1995, **28**, 366–367.
30. Young, R. A., Introduction to the Rietveld method. The Rietveld method. In *International Union of Crystallography, Monographs on Crystallography*, ed. R. A. Young. Oxford University Press , 1993, pp. 1–38.
31. DMPLOT is ancillary to DBWS-9411, Marciniak, H., Diduszko, R. Contact Dr. Henryk Marciniak, High Pressure Research Center, ul. Sokolowska, 01-142 Warsaw, Poland, private communication.
32. *International Tables for X-Ray Crystallography*, *Vol II*, ed. N. F. M. Henry and K. Lonsdale. The KYNOCH Press, 1965, p. 99.
33. Azavant, P. and Lichanot, A., X-ray scattering factors of oxygen and sulfur ions: an *ab initio* Hartree–Fock calculation. *Acta Cryst*, 1993, **A49**, 91–97.
34. Caglioti, G., Paoletti, A. and Ricci, F. P., Choice of collimators for a crystal spectrometer for neutron diffraction. *Nucl. Instrum.*, 1958, **3**, 223–228.
35. Dollase, W. A., Correction of intensities for preferred orientation in powder diffractometry: application of the March model. *J. Appl. Cryst.*, 1986, **19**, 267–272.
36. Sparks, C. J., Kumar, R., Specht, E. D., Zschack, P., Ice, G. E., Shiraishi, T. *et al.*, *Adv. X-Ray Anal.*, 1992, **35**, 57–62.
37. Hamilton, W. C., Significance tests on the crystallographic *R* factor. *Acta Cryst.*, 1965, **18**, 502–510.
38. Marsh, R. E., Some thoughts on choosing the correct space group. *Acta Cryst.*, 1995, **B51**, 897–907 (and reference therein).
39. Young, R. A. and Sakthivel, A., Bimodal distribution of profile-broadening effects in Rietveld refinement. *J. Appl. Cryst.*, 1988, **21**, 416–425.
40. Zhou, Y., Microstructural development of sintered ZrO_2–CeO_2 ceramics. *Ceram. Int.*, 1991, **17**, 343–346.
41. Santoro, A., Marezio, M., Roth, R. S. and Minor, D., Neutron powder diffraction study of the structures of $CeTaO_4$, $CeNbO_4$, and $NdTaO_4$. *J. Solid State Chem.*, 1980, **35**, 167–175.
42. Sellar, J. R., Disorder, superlattice canting and chiral domains in zirconia-niobia ceramic alloys. *Acta Cryst.*, 1999, **A55**, 220–227.
43. Pitschke, W., Hermann, H. and Mattern, N., The influence of surface roughness on diffracted X-ray intensities in Bragg–Brentano geometry and its effect on the structure determination by means of Rietveld analysis. *Powder Diffraction*, 1993, **8**, 74–83.
44. Pitschke, W., Mattern, N. and Hermann, H., Incorporation of microabsorption corrections into Rietveld analysis. *Powder Diffraction*, 1993, **8**, 223–228.
45. Thompson, P., Cox, D. E. and Hastings, J. B., Rietveld refinement of Debye–Scherrer Synchroton X-ray data from Al_2O_3. *J. Appl. Cryst.*, 1987, **20**, 79–83.
46. Young, R. A. and Desai, P., Crystallite size microstrain indicators in Rietveld refinement. *Archiwum Nauki o Materialach*, 1989, **10**, 71–90.
47. Delhez, R., de Keijser, T. H., Langford, J. I., Louër, D., Mittemeijer, E. J. and Sonneveld, E. J., Crystal imperfection broadening and peak shape in the Rietveld method. *The Rietveld Method*. In *International Union of Crystallography, Monographs on Crystallography*, ed. R. A. Young. Oxford University Press, 1993 (pp. 132–166).
48. Paiva-Santos, C. O., Gouveia, H., Las, W. C. and Varela, J. A., Gauss-Lorentz size-strain broadening and cell parameters analysis of Mn doped SnO_2 prepared by organic route. *Mater. Struct.*, 1999, **6**, 1–4.